Supplementary Information
for

Development of a sub-ppb resolution methane sensor using a GaSb-based DFB diode laser near 3270 nm for fugitive emissions measurement

Jalal Norooz Oliaee,[1*] Nicaulas Sabourin,[2] Simon Festa-Bianchet,[3] James A. Gupta,[2] Matthew R. Johnson,[3] Kevin A. Thomson,[1] Greg J. Smallwood,[1] and Prem Lobo[1]

[1] Metrology Research Centre, National Research Council Canada, Ottawa, Ontario K1A 0R6, Canada

[2] Advanced Electronics and Photonics Research Centre, National Research Council Canada, Ottawa, Ontario K1A 0R6, Canada

[3] Department of Mechanical and Aerospace Engineering, Carleton University, Ottawa, Ontario K1S 5B6, Canada

Spectral probing region

Figure S1 illustrates the line intensities of vibration-rotation transitions of methane from HITRAN2016 database at 296 K.[1] The strongest absorption band of methane arises from its ν_3 fundamental vibration with a central frequency of 3019 cm^{-1} (3.31 μm). The strongest transition of the ν_4 band, centered around 1306 cm^{-1} (7.66 μm), is about half as strong as the strongest transition of the ν_3 band. The $2\nu_3$ band is about two orders of magnitude weaker than the ν_3 band.

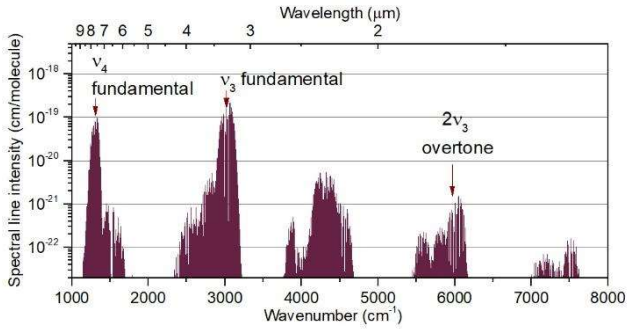

Figure S1. Line intensities of vibration-rotation transitions of methane from HITRAN2016 at 296 K on logarithmic scale.

A close-up of the ν_3 band of methane is shown in Figure S2 with R(3) transitions that are probed in this work shaded in gray.

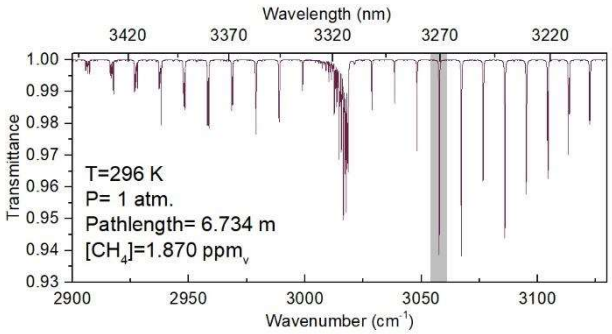

Figure S2. Transmission spectrum of ν_3 band of 1.87 ppm_v methane in air at T=296 K and P=1 atm. with an absorption path length of 6.734 meters. The shaded region shows blended R(3) transitions probed in this study.

The R(3) transitions of methane in the ν_3 band are labelled by their lower state symmetry species as A_2, F_2, and F_1 as shown in the spectrum in Figure S3 (solid line) and Table S1. Although discrepancies between HITRAN pressure broadening data for the R(3) transition of methane and those at reduced pressures have been reported,[2] the HITRAN2016 parameters have been used in producing the high resolution spectrum in Figure S3. At atmospheric pressure, the R(3) group of transitions resemble a single absorption feature (Figure S3, dashed line), but it should

be noted that the lineshape function for the blended transition is not fully symmetric such as a single Lorentzian or Voigt lineshape.

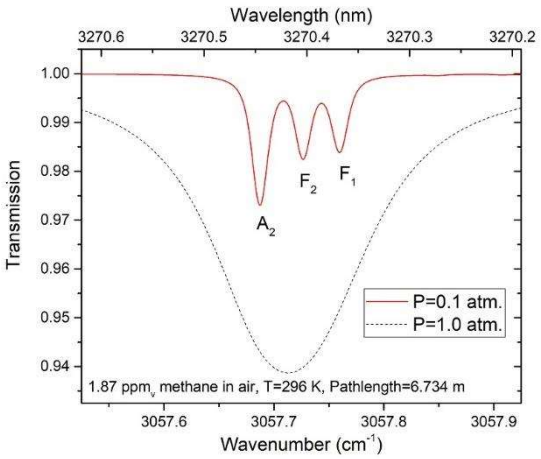

Figure S3. High resolution transmission spectrum of R(3) manifold lines of methane at 0.1 atm. labelled by their lower state symmetry species (solid line) along with pressure-broadened spectrum at atmospheric pressure (P=1.0 arm., dashed line). The spectra are calculated based on HITRAN2016 parameters at T=296 K, and path length=6.734 meters for 1.870 ppm_v concentration, and a Voigt lineshape.

Table S1. Line position and intensities of methane

Transition	Line position (cm^{-1})	Line intensity (cm/molecule)
R(3) A2	3057.687423	2.106×10^{-19}
R(3) F2	3057.726496	1.260×10^{-19}
R(3) F1	3057.760735	1.260×10^{-19}

R(3) manifold lines of methane within the ν_3 band probed in this study. Values reported from HITRAN2016.

Multi-pass cell design

A ray-tracing program has been developed in MATLAB to guide the design of the multi-pass cell (MPC). The program is based on three-dimensional analytical expressions for mirror surfaces and propagation wave vectors to calculate reflected wave vectors. Therefore the calculations do not assume the paraxial approximation and illustrate beam focusing and refocusing as the laser goes through each pass. A hundred initial wave vectors were used to sample the laser beam cross section and to illustrate the beam envelope trajectory within the cell (Figure S4).

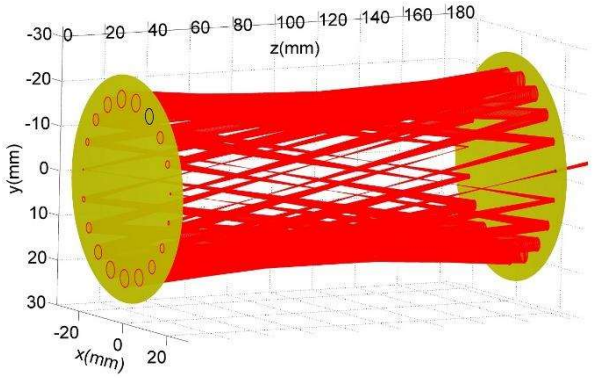

Figure S4. Calculated beam trajectory inside the multi-pass cell assuming a collimated beam with a circular cross-section of 3.5 mm in diameter. The black circle on the back of the mirror on the left indicates the in-coupling laser beam.

Realistic but conservative laser beam parameters were input to the program. A collimated elliptical beam cross-section with diameters ($1/e^2$) of 4.2 mm and 2.0 mm for fast and slow axes, respectively, were used. The mirror separation was varied to produce uniformly distributed spot centers while ensuring the laser spots are far from overlapping (Figure S5). As illustrated in Figure S5a, the output beam diameter is relatively small compared to the out-coupling hole reducing the risk of beam clipping in case of slight beam steering. The positions of the in- and out-coupling holes are dictated by the requirements of maintaining a circular pattern while keeping one of the injection angles equal to zero (θ_y=0°), so that only one injection angle adjustment is required to align the MPC.

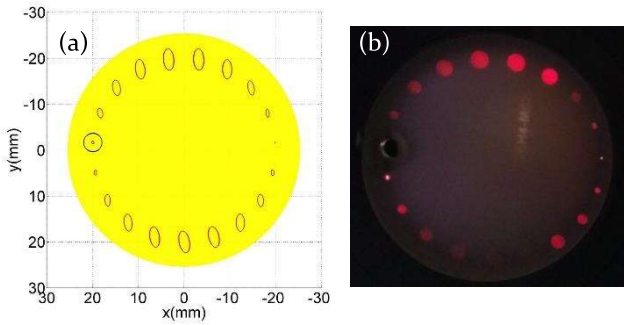

Figure S5. (a) Calculated spot pattern on the back/far mirror (view along –z direction). The black circle indicates the out-coupling hole (∅ 4mm). (b) Spot pattern as seen from the back of the far mirror when a 650 nm collimated laser was used for illustration purposes. The program correctly produces the size of the spots as the laser beam is focused and refocused repeatedly upon each reflection.

Sensor calibration

The mass flow controllers (MFCs) were programmed to produce a range of flow rates corresponding to methane concentrations from 1.5 to 40 ppm_v in a randomized sequence, as shown in Figure S6.

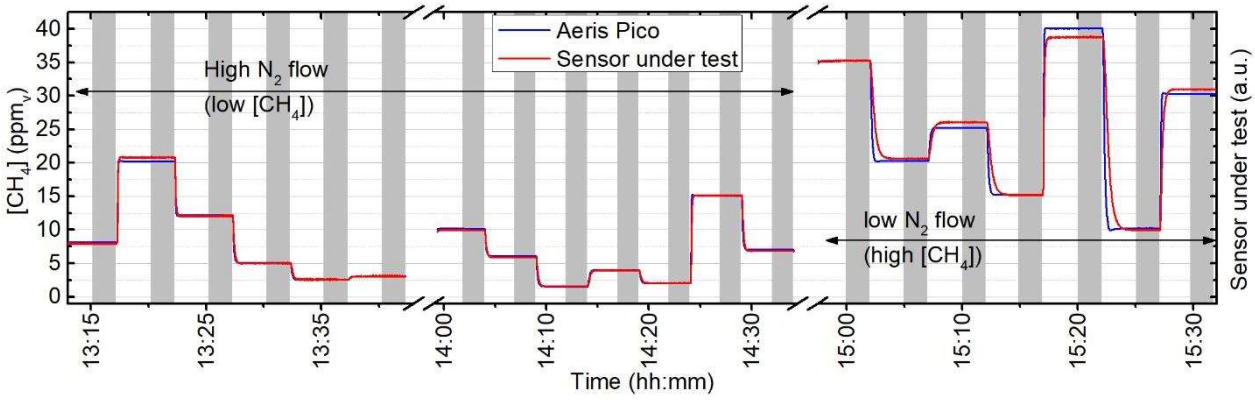

Figure S6. Methane gas concentration time series produced by controlling flow rates from a certified cylinder of 50 ppm methane in nitrogen balance and an ultra-high purity nitrogen gas cylinder. Reference measurements from a commercial gas analyzer (Aeris Pico, blue trace) as well as response of the sensor presented in this work in terms of area under the quadrature *2f/1f* signal (red trace) are shown. Gray areas show stable intervals used for averaging.

To maintain the MFCs within their calibration range, a high flow rate and a low flow rate for nitrogen gas (44.0 slpm and 9.5 slpm) were chosen to produce low and high methane concentration setpoints, respectively. Each concentration setpoint was maintained for five minutes to allow for complete mixing within the enclosure, with the data from the last two minutes used to calculate an average concentration for calibration. The lower total flow rates associated with the higher methane concentration setpoints resulted in a lower gas exchange rate through the calibration enclosure volume which can be seen in the slow rise/fall on the right side of Figure S6. Consequently, it should be noted that the rise/fall times in Figure S6 are not a reflection of the sensor's response time but rather of constraints in the MFC's calibration ranges.

Concentration of calibration gas was obtained by

$$[CH_4] = \frac{Q_{CH_4}}{Q_{N_2} + Q_{CH_4}} \times [CH_4]_{Cal.Gas} \qquad \text{Eq. 1}$$

where Q_{N_2} and Q_{CH_4} are the flow rates from the ultra-high purity nitrogen cylinder and the certified 50 ppm_v methane in nitrogen balance cylinder, respectively, and $[CH_4]_{Cal.Gas} = 50.0 \times 10^{-6}$. The uncertainty in calibration gas methane concentration was propagated from flow uncertainties reported by the MFCs calibration uncertainties and the stated uncertainty of the certified calibration gas cylinder of 50.0 ± 0.5 ppm, as

$$\Delta[CH_4] = \sqrt{u_{Q_{CH_4}}^2 \Delta Q_{CH_4}^2 + u_{Q_{N_2}}^2 \Delta Q_{N_2}^2 + u_{Cal.Gas}^2 \Delta[CH_4]_{Cal.Gas}^2} \qquad \text{Eq. 2}$$

In which

$$u_{Q_{CH_4}} = \frac{Q_{N_2}}{\left(Q_{CH_4} + Q_{N_2}\right)^2} \times [CH_4]_{Cal.Gas}$$

$$u_{Q_{N_2}} = -\frac{Q_{CH_4}}{\left(Q_{CH_4} + Q_{N_2}\right)^2} \times [CH_4]_{Cal.Gas}$$

$$u_{Cal.Gas} = \frac{Q_{CH_4}}{Q_{CH_4} + Q_{N_2}}$$

For all concentration setpoints the propagated relative uncertainty is very close to 1% with the uncertainty of the certified calibration gas cylinder being the dominant contributor.

Response in the ppb-level range

The response of the sensor to ppb-level changes in the background methane concentration was demonstrated by adding a low flow from a standard 2 ppm methane-in-nitrogen cylinder to a high flow of laboratory compressed air. The laboratory compressed air contained a consistent elevated concentration of methane which on the day of running the test measured 3.472±0.017 ppm_v. Concentration steps in the range of 1-10 ppb_v were produced by diluting laboratory compressed air with volumetric ratios of 75:0.05 to 75:0.5. For concentration step changes in the 10-15 ppb_v, a mix ratio of 50:0.3 to 50:0.5 was used. Sections of methane concentration timeseries recorded with the present sensor running at 1 Hz is shown in Figure S7. Averaging intervals were kept short (< 1 minute) due to variability of methane concentration in the air stream. Positive and negative step changes corresponding to the same absolute value were grouped together and were used to assess the response of the sensor to these ppb-level step changes as shown in Figure 7 of the main article.

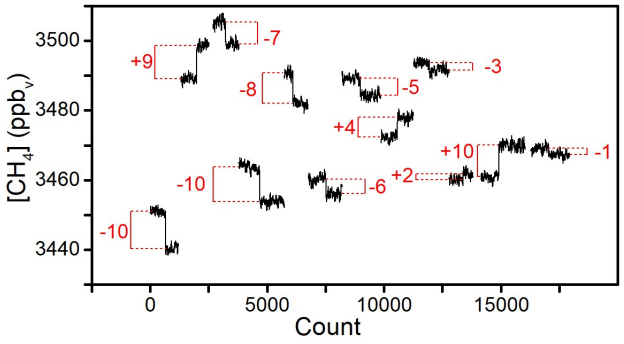

Figure S7 Sections of methane concentration timeseries recorded at 1 Hz showing ppb-level step changes in background methane concentration. The labels associated with each step (in red) correspond to step changes obtained from MFC setpoints in ppb_v.

Direct absorption spectrum fit model

The absorption model is based on HITRAN formulation presented in section A.2. of Ref. [3] assuming a cubic background form, and a Lorentzian lineshape with molecular transition parameters taken from HITRAN2016. A Lorentzian lineshape function has been assumed since the Doppler line broadening is negligible compared to Lorentz broadening for the R(3) manifold transitions of methane around 3057.7 cm^{-1} ($\alpha_L/\alpha_D \cong 13; T = 296\ K, P = 1\ atm$). Vibrational-rotational transitions of water and methane from 3054.0 cm^{-1} to 3061.0 cm^{-1} are included in the absorption model. The detector output signal from five successive DAS scans are averaged every second and fitted to

$$V(x_n) = (b_0 + b_1 \cdot x_n + b_2 \cdot x_n^2 + b_3 \cdot x_n^3) \times e^{-\frac{[X_i]P}{k_B T} \cdot l \cdot \sum_i \tau_i} + V_0. \quad \text{Eq. 3}$$

where $V(x_n)$ is the detector output signal (in Volts); x_n represents the channel count of the acquired signal that is related to time elapsed since start of the scan via $t_n = x_n/f_S$ where f_S is the sampling frequency; V_0 is the detector signal level below the TDL threshold current measured for each DA spectrum; τ_i is the wavenumber-dependent optical thicknesses for species i (i=1, 2 for methane and water, respectively); P and T are measured air pressure and temperature (in Pa and in Kelvin, respectively), $[X_i]$ represents gas mixing ratios (the product of which with total pressure P provides the partial pressure of species i, p_i); k_B is the Boltzmann constant (in J/K), and l is the absorption path length (in cm) estimated from MPC design parameters. By assuming a Lorentzian lineshape function, τ_i is expressed by:

$$\tau_i = \sum_j \frac{S_{ij}}{I_i} \frac{1}{\pi} \frac{\gamma_{ij}}{(\upsilon - \upsilon_{ij})^2 + {\gamma_{ij}}^2}, \quad \text{Eq. 4}$$

where the ij subscripts correspond to the j^{th} transition of the i^{th} species; S_{ij} are spectral line intensities (in $cm/molecule$) that are weighted according to the natural terrestrial isotopic abundances, I_i, (0.988274 for $^{12}CH_4$); ν_{ij} are transition wavenumbers; and γ_{ij} are the pressure broadening half-widths (in cm^{-1}) with contributions from self-broadening, b_{self}, and air-broadening, b_{air}, coefficients, as

$$\gamma_{ij} = \left(\frac{T_{ref}}{T}\right)^{n_{air}} \left[b_{air}(P - p_i) + b_{self}(p_i)\right], \quad \text{Eq. 5}$$

where n_{air} is the temperature dependence coefficient of air-broadening and $T_{ref} = 296\ K$ is the HITRAN reference temperature. The temperature dependence of the line intensities has been accounted for according to

$$S_{ij}(T) = S_{ij}(T_{ref}) \frac{Q(T_{ref})}{Q(T)} \times \frac{\exp(-c_2 E''/T)}{\exp(-c_2 E''/T_{ref})} \times \frac{1 - \exp(c_2 \nu_{ij}/T)}{1 - \exp(c_2 \nu_{ij}/T_{ref})}, \quad \text{Eq. 6}$$

where $Q(T)$ is the partition function interpolated from HITRAN2016; E'' is the lower state energy for each transition and $c_2 = hc/k = 1.4387769\ cm.K$ is the second radiation constant. A quadratic expression has been used for mapping data channels to the wavenumber scale

$$\upsilon = \upsilon_0 + \eta_1 \cdot x_i + \eta_2 \cdot x_i^2, \quad \text{Eq. 7}$$

and the background laser radiation is described by a 3rd order polynomial as is evident in Eq. 3. Pressure shifts are not included in the model since they are negligible compared to the width of pressure-broadened absorptions. At atmospheric pressures, the R(3) manifold lines of methane are not rotationally resolved and have an effective FWHM of about 0.16 cm^{-1} (4.8 GHz). This necessitates the use of a good set of initial fit parameters that are determined with known laser tuning parameters, especially in the case of dry sample gases where the only prominent spectral feature in the laser coverage range is the methane absorption. The constructed model has a total of nine floating parameters and was fitted to the observed spectra with employing the LabView Levenberg-Marquardt non-linear least squares fitting procedure to find best fit parameters including the methane gas concentration.

Linear fits of WMS metrics

The plot of WMS metrics as a function of calibration gas methane concentrations was fitted to a linear expression for each metric for the entire range of produced concentrations as well as fits for up to 8 ppm_v only. The results of the fits are presented in Table S2.

Table S2. Linearity of WMS metrics

metric	pk-pk X_{2f}		pk $Q(2f\text{-}2f_0)$		pk $Q(2f/1f\text{-}2f_0/1f_0)$	
concentration range (ppm)	1.5-8	1.5-40	1.5-8	1.5-40	1.5-8	1.5-40
slope	$1.725(22)\times10^{-2}$	$1.019(56)\times10^{-2}$	$1.100(14)\times10^{-2}$	$6.38(37)\times10^{-3}$	$2.332(16)\times10^{-2}$	$2.877(96)\times10^{-2}$
intercept	$5.3(1.1)\times10^{-3}$	$5.04(99)\times10^{-3}$	$2.64(70)\times10^{-3}$	$3.21(64)\times10^{-2}$	$4.2(7.5)\times10^{-4}$	$-4.4(1.7)\times10^{-2}$
R^2	0.9989	0.9482	0.9988	0.9438	0.9997	0.9803
Residual sum of squares	1.41×10^{-5}	1.41×10^{-2}	6.21×10^{-6}	6.03×10^{-3}	7.21×10^{-6}	4.13×10^{-2}

metric	Area $Q(2f\text{-}2f_0)$		Area $Q(2f/1f\text{-}2f_0/1f_0)$	
slope	$1.310(11)\times10^{+1}$	8.69(37)	$2.982(19)\times10^{+1}$	$3.087(30)\times10^{+1}$
intercept	3.29(54)	$3.19(64)\times10^{+1}$	-1.31(92)	-2.5(5.3)
R^2	0.9995	0.9693	0.9997	0.9983
Residual sum of squares	3.67	$5.94\times10^{+3}$	$1.06\times10^{+1}$	$4.14\times10^{+3}$

Values in parentheses are standard deviations obtained from the fits.

References

(1) Gordon, I. E.; Rothman, L. S.; Hill, C.; Kochanov, R. V.; Tan, Y.; Bernath, P. F.; Birk, M.; Boudon, V.; Campargue, A.; Chance, K. V.; et al. The HITRAN2016 Molecular Spectroscopic Database. *J. Quant. Spectrosc. Radiat. Transf.* **2017**, *203*, 3–69. https://doi.org/10.1016/j.jqsrt.2017.06.038.

(2) Manne, J.; Bui, T. Q.; Webster, C. R. Determination of Foreign Broadening Coefficients for Methane Lines Targeted by the Tunable Laser Spectrometer (TLS) on the Mars Curiosity Rover. *J. Quant. Spectrosc. Radiat. Transf.* **2017**, *191*, 59–66. https://doi.org/10.1016/j.jqsrt.2017.01.035.

(3) Rothman, L. S.; Rinsland, C. P.; Goldman, A.; Massie, S. T.; Edwards, D. P.; Flaud, J.-M.; Perrin, A.; Camy-Payret, C.; Dana, V.; Mandin, J.-Y.; et al. The HITRAN Molecular Spectroscopic Database and HAWKS (HITRAN Atmospheric Workstation): 1996 Edition. *J. Quant. Spectrosc. Radiat. Transf.* **1998**, *60* (5), 665–710. https://doi.org/http://dx.doi.org/10.1016/S0022-4073(98)00078-8.